Patterned flexoelectric instability in a bent-core nematic liquid crystal

ARTICLE *in* SOFT MATTER · JANUARY 2012

Impact Factor: 4.03 · DOI: 10.1039/C1SM06870A

3 AUTHORS, INCLUDING:

Pramod Tadapatri
Raman Research Institute
9 PUBLICATIONS **76** CITATIONS
SEE PROFILE

K. S. - Krishnamurthy
Centre for Nano and Soft Matter Sciences (f…
41 PUBLICATIONS **239** CITATIONS
SEE PROFILE

Soft Matter

Cite this: *Soft Matter*, 2012, **8**, 1202

www.rsc.org/softmatter

PAPER

Patterned flexoelectric instability in a bent-core nematic liquid crystal

Pramod Tadapatri,[a] Kanakapura S. Krishnamurthy*[a] and Wolfgang Weissflog[b]

Received 30th September 2011, Accepted 26th October 2011
DOI: 10.1039/c1sm06870a

We examine here the Bobylev–Pikin flexoelectric instability in an initially planar monodomain of a bent-core nematic liquid crystal, which is negative in conductivity and dielectric anisotropies. Experiments employing dc excitation reveal the domain density to be linear in field, as predicted; however, the instability threshold has a negative temperature coefficient indicating the effective flexomodulus as nonquadratic in order parameter. The dc threshold is also determined as a function of simultaneously acting ac voltage; a theoretical fit is found for the data taking into account elastic anisotropy, whereby the relevant flexoelectric and elastic parameters are estimated. Remarkable morphological changes occur under an increasing field. Half-strength disclinations of opposite topological charge evolve within the flexostructure rendering the wavevector orientation degenerate in the layer plane. Dipolar and quadrupolar topological defect patterns, akin to the singularities in cholesteric fingerprint texture, lead finally to fan like objects. The morphological equivalence between the periodic flexoelectric state and a layered lattice as realized here is attributable to a much lower energy of bend type distortion compared to splay, unlike in a calamitic.

1 Introduction

The reduced symmetry of bent-core (BC) molecules, once regarded unfavourable to mesophase formation, has turned out to be the key element in producing several radically new forms of liquid crystalline aggregation, the so-called banana phases Bn (n = 1, …, 8), not found in straight-core (calamitic) systems.[1–3] Studies on BC mesogens in the last fifteen years, triggered indubitably by the discovery of achiral molecules exhibiting layer chirality and polar switching,[4,5] have led to many-sided extension of the field of mesomorphism. While banana phases are obviously the major part in this advance, even the bent-core nematic (BCN) phase has several novel aspects that set it apart from the calamitic nematic (CN). In a recent discussion on the macroscopic and symmetry properties of nonpolar nematics composed of achiral molecules, the BCN phase is recognized as possibly possessing an octupolar or tetrahedratic order besides the usual quadrupolar order, and, therefore, as belonging to the D_{2d} symmetry rather than the familiar $D_{\infty h}$ symmetry of the CN;[6] while optically the tetrahedratic nematic mimics the CN, it is capable of such extraordinary properties as are unobservable in the latter; for example, it may exist in ambidextrous helical ground states, exhibit Lehmann-like rotations, allow second harmonic generation and respond anomalously to dielectric torques. Thus, the previous experimental finding in some BCNs of spontaneous formation of chiral domains of opposite handedness[7–11] seems to find an explanation in the tetrahedratic order. Experiments on BCNs have also shown several other uncommon features: Unlike in most CNs, there is ample evidence of short range smectic order existing throughout the nematic range of BC compounds, even in the absence of an underlying smectic (Sm) phase.[12–16] Secondly, the anisotropic character of material properties differs for CNs and BCNs. For instance, the inequality between splay (k_{11}), twist (k_{22}) and bend (k_{33}) elastic moduli in calamitics is often expressible as $k_{33} > k_{11} > k_{22}$,[17,18] whereas in some BCNs it is found that $k_{11} > k_{33}$,[19–22] while k_{22}, as determined in one case recently,[22] may remain the lowest. Similarly, rotational viscosity (γ_1) is an order more for BCNs compared to CNs, and also the viscous relaxation appears to be a two-step process.[19,22,23]

The uncommon behaviour of BCNs extends also to flexoelectric phenomena that form the subject of this paper. In both direct and converse flexoelectric ('flexo', for brevity) experiments employing flexible electrodes, a BC nematic has been found to show giant values (~nC m^{-1}) for the bend flexocoefficient e_b;[24–26] in converse flexo-studies on BCNs using rigid electrodes, however, only conventional e_b values (~pC m^{-1}) have been obtained;[27,28] to resolve this discrepancy, a model of nonpolar molecular clusters showing quadrupolar flexoeffect has been advanced.[28] However, energy conservation arguments seem to disallow giant values of flexomoduli;[29] a radically new explanation of the giant flexoeffect is based on monopole contribution in nematics confined between flexible electrodes and analogous to bilayer lipid membranes.[30] A particularly intriguing question that prompted this study relates

[a]*Centre for Soft Matter Research, P. O. Box 1329, Jalahalli, Bangalore, 560013, India. E-mail: murthyksk@gmail.com*
[b]*Martin-Luther-Universität Halle, Institut für Physikalische Chemie, von-Danckelmann-Platz 4, 06120 Halle (Saale), Germany*

to earlier observations[7,8,31] of a Sm-like fan texture evolving within some planar BCN layers exposed to increasing dc fields; here the initial stripe domains along the easy axis develop, *via* a myelinic texture, into fan-shaped objects. Our detailed studies of these morphological transformations now confirm that the initial domains are due to the well-known Bobylev–Pikin instability or the variable grating mode (VGM),[32–37] and it is through a combination of the VGM and randomization of the local wavevector that the fans form. We present and discuss here our observations on the VGM mode in a BCN under increasing control parameter.

2 Experimental section

The material investigated, 4-chlororesorcinol bis[4-(4-*n*-undecanoyloxybenzoyloxy) benzoate] (11Cl), belongs to the series with the following chemical structure. It was first synthesized by Weissflog *et al.*,[8] who employed optical, electro-optical, NMR and X-ray methods to characterize the observed phases and reported the phase sequence of 11Cl as Cr 88 °C (M 73 °C) N 95 °C I, with Cr, N and I denoting respectively the crystal, nematic and isotropic phases; M is an optically isotropic 'banana' phase monotropically derived from the N phase. For the sample used in this study, the transition temperatures from optical microscopy were lower than the reported values by 2–3 °C, with the N–I transition temperature T_{NI} being 92 °C. We indicate the sample temperature T (K) by its reduced value $T^* = T/T_{NI}$.

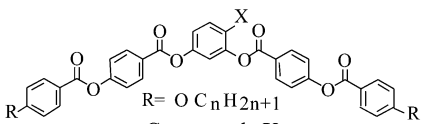

Compound nX

The sample cells used for optical studies were sandwich type, constructed of indium tin oxide (ITO) coated glass plates. The planar alignment was secured by spin coating the ITO electrodes with polyimide and then buffing unidirectionally the coated surfaces on a tissue paper. The rubbing direction and the layer normal define the reference axes x and z, respectively. Mylar spacers, heat-sealed to the electrodes through cooling from ~250 °C under a uniform pressure, determined the cell gap, which was measured interferometrically. For optical observations, a Carl-Zeiss Axio Imager.M1m polarizing microscope equipped with an AxioCam MRc5 digital camera was used. The sample temperature T was maintained to an accuracy of ±0.1 °C by an Instec HCS402 hot-stage connected to an STC200 temperature controller. The voltage source was a Stanford Research Systems DS345 function generator coupled to a FLC Electronics voltage amplifier (model A800). The applied voltage was measured with a Keithley-200 multimeter.

Most of the studies were conducted at $T^* = 0.989$. From our dielectric dispersion studies (see ref. 20 for experimental details), the principal components of static permittivity at this temperature are $\varepsilon_{\parallel} = 4.550$ and $\varepsilon_{\perp} = 5.528$, where the subscripts denote the direction relative to the nematic director.

3 Results and discussion

3.1 Flexoelectric domains in a static field

A thin planarly aligned nematic layer of 11Cl subjected to a quasistatically increasing dc field bifurcates into a patterned state above a well defined voltage threshold V_c, displaying parallel bands along the initial alignment direction x, with periodicity along y, as in Fig. 1. In Fig. 1a, along the extinction bands parallel to x, the director is confined exclusively to the xz plane. The optical path retardation along these bands, determined with crossed polarizers turned to the diagonal position and using a tilt compensator, reduces with increasing voltage, reaching a near constant value for $V = 1.2\ V_c$, as seen in Fig. 2. Clearly, along these bands, the molecular tilt averaged over the layer thickness is a sigmoid-like function of V. Between the extinction bands, the birefringence colour increases toward the centre where the colour is first order orange, which is nearly the same as that of the sample in the field-free state. Thus, the director is turned exclusively in the layer plane along the central line between the dark bands. That this turn is opposite for the two bright bands flanking a dark band is indicated by the texture of alternating colour bands in Fig. 1b observed under slightly uncrossed polarizers. These features suggest that the pattern in Fig. 1 is due to the Bobylev–Pikin (BP) instability,[34,35] which is a volume flexoelectric effect arising in layers with strong planar anchoring at the substrates. It involves a two-dimensional deformation characterized by the director deviation away from x, by an angle θ in the xz-plane and φ in the xy-plane. The director distribution is defined by $\theta = \theta_o \cos(qy) \cos(\pi z/d)$ and $\varphi = \varphi_o \sin(qy) \cos(\pi z/d)$, where d is the sample thickness and q, the angular wavenumber, is related to the spatial period of the pattern λ or the domain width w by $q = 2\pi/\lambda = \pi/w$. This modulated structure may be considered as associated with chirality,[38] as indicated in Fig. 3 showing a plot of normalized angular deviations (θ/θ_o) and (φ/φ_o) along y, in the sample midplane. The sense of this chirality changes on reversing the field. Thus the BP transition involves breaking of chiral symmetry and is expectedly polarity sensitive.

Instead of applying a slowly increasing field, when a field exceeding the threshold is suddenly applied to the sample, the initial texture under crossed polarizers consists of interconnected

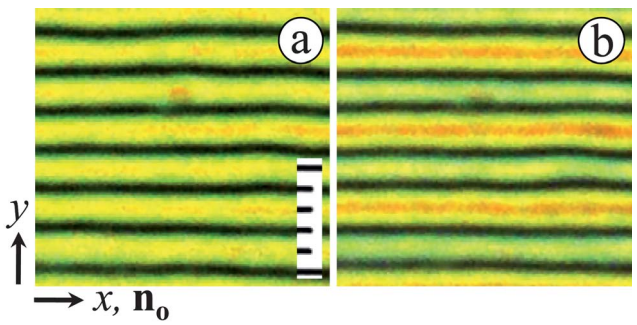

Fig. 1 Flexoelectric domains in a 5.5 μm thick layer of nematic 11Cl; $T^* = 0.989$, $V = 1.088\ V_c$. (a) Crossed polarizers with their axes along xx and y. Along the extinction bands parallel to x, the director is confined to the xz plane. (b) Slightly uncrossed polarizers; on either side of near-extinction bands, the interference colours differ due to opposite azimuthal deviations of the director; 2 μm scale div.

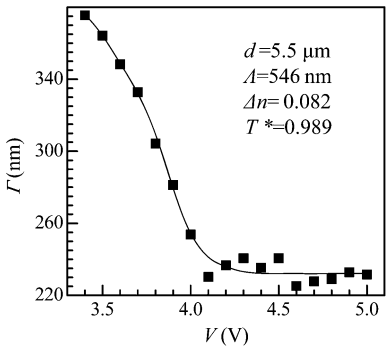

Fig. 2 Optical path difference along a line of maximum tilt angle θ_o in the (θ, φ) flexoelectric pattern as a function of applied dc voltage. Δn is the birefringence for wavelength Λ.

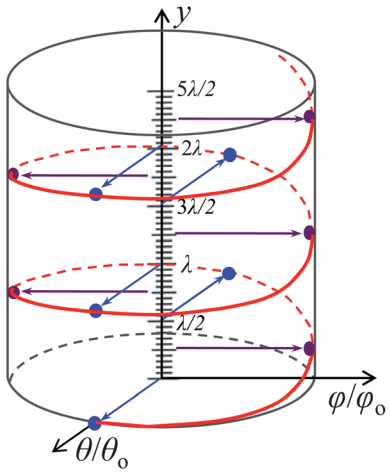

Fig. 3 Variation of normalized θ and φ along the y axis, in the midplane corresponding to $z = d/2$. Blue and purple dots represent, respectively, pure θ and φ deviations.

crosslike domains, as shown in Fig. 4a. With passage of time, the diagonal regions of crosslike domains with the same sense of azimuthal deviation join to first produce linear oblique domains as depicted in Fig. 4b–f, which eventually straighten into the usual longitudinal geometry of the BP domains with the wave vector along y. This evolution process gradually slows down, with the initial stages (a–d) occupying far less time relative to the final stages (d–f) in which the edge dislocations are progressively eliminated. It is to be noted that the crosslike domains in Fig. 4a are not an indication of any surface polarization effect such as found in homeotropic samples of cyanobiphenyls.[39] Very careful studies of z-stacked images revealed this texture to be not localized at either substrate; nor did reversal of the field change the contrast of the image or shift in the focal plane. Secondly, to obtain the (θ, φ) modulation at the substrate, one has to assume weak polar and azimuthal anchorings, which seem improbable under planar alignment with polyimide treatment. Moreover, the VGM observed (see Section 3.3) is very typical of the volume flexoeffect under strong anchoring. Finally, the type of singular lines and fingerprint texture that occur (see Section 3.4) are reasonably to be expected as volume effects.

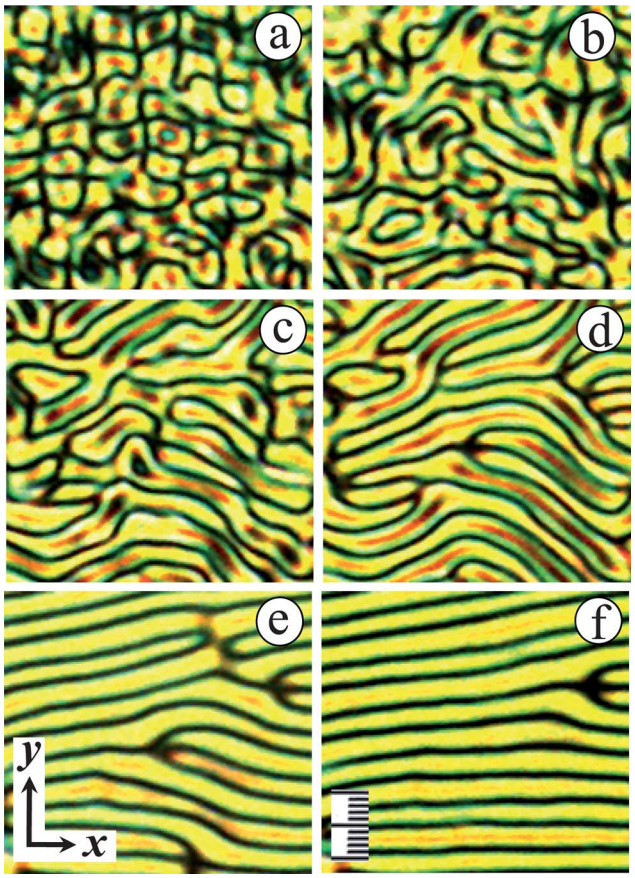

Fig. 4 Time series of orientational patterns in an initially planar sample excited by a dc field, recorded under crossed polarizers with their axes along (x, y), showing the transformation of Maltese crosses into stripes. Separation between successive frames is 10 s for (a–d) and 100 s for (d–f). (a) Network of domains with dark crosses 5 s after a sudden application of 1.15 V_c. (b–d) The diagonal regions of crosslike domains with the same sense of azimuthal deviation joining to produce linear oblique domains. (e and f) Gradual formation of the Bobylev–Pikin domains with the wave vector along y. This evolution process gradually slows down, with the initial stages (a–d) occupying far less time relative to the final stages (d–f) in which the edge dislocations are progressively eliminated. $T^* = 0.989$; 1 μm scale div.

The threshold voltage and wavenumber of the BP instability are given by:[36]

$$V_c = \frac{2\pi k}{e^*(1+\mu)}, \quad \mu = \frac{\varepsilon_0 \varepsilon_a k}{e^{*2}} \tag{1}$$

$$q_c = \frac{2\pi}{\lambda_c} = \frac{\pi}{w_c} = \frac{\pi}{d}\sqrt{\frac{1-\mu}{1+\mu}} \tag{2}$$

Here k is the elastic modulus under one-constant approximation, e^* is the difference $|e_s - e_b|$ with e_s and e_b as the splay and bend flexocoefficients, and λ_c and w_c are the critical or threshold values of λ and w.

From eqn (1) and (2), we derive

$$e^* = \frac{\varepsilon_0 \varepsilon_a V_c}{\pi\left(1 - \frac{d^2}{w_c^2}\right)} \tag{3}$$

and

$$\frac{k}{e^{*2}} = \frac{(w_c^2 - d^2)}{\varepsilon_0 \varepsilon_a (w_c^2 + d^2)} \quad (4)$$

Thus, in principle, it is possible to extract both k and e^* using the experimental values of ε_a, V_c and w_c. For instance, with a 5.5 μm thick sample of 11Cl, we found $w_c = 4.6$ μm and $V_c = 3.5$ V. From our dielectric data, $\varepsilon_a = 0.978$ at $T^* = 0.989$. Using eqn (3) and (4), we arrive at $e^* = 22.46$ pC m^{-1} and $k = 10.29$ pN. Both these values appear to be overestimates, with the elastic modulus in particular being at least twice the value to be expected from measurements on similar BCNs like 12CN and 9CN.[19,20] The discrepancy, as we shall see in the next section, is mainly due to the assumption of elastic isotropy.

$$V_{dc}^2 = \frac{k^2\pi^2(1+P)}{Pe^{*2}(1-|\mu|)}\left(\frac{(1+P)}{(1-|\mu|)} + \frac{V_{ac}^2}{V_0^2}\right); P = \sqrt{1+(1-|\mu|)\frac{V_{ac}^2}{V_0^2}} \quad (5)$$

In this equation, electric field gradients that contribute to quadrupolar flexoelectric terms are neglected. It may be noted in Fig. 5 that, as V_{ac} increases, the values of V_{dc} obtained from eqn (5) using the aforementioned experimental values of k, e^* and ε_a fall increasingly short of the observed values. A major source of this discrepancy is to be traced to the assumption of elastic isotropy in deriving eqn (1), (2) and (5). The BP deformation comprises both splay and twist components of which the splay is usually more energy demanding ($k_{11} > k_{22}$). Taking this inequality into account, it has been shown that[42]

$$V_{dc}^2 = \frac{k_{11}k_{22}\pi^2}{Pe^{*2}}\left(1 + b\frac{\mu+P}{1-b|\mu|}\right)\left(1 + a\frac{\mu+P}{1-b|\mu|} + \frac{V_{ac}^2}{V_0^2}\right), \text{with } V_0 = \pi\sqrt{\frac{k_{11}}{\varepsilon_0|\varepsilon_a|}},$$

$$P = \sqrt{\frac{1-b|\mu|}{ab}\left(1+\frac{V_{ac}^2}{V_0^2}\right) + \frac{|\mu|}{b}}; a = \frac{1}{2} + \frac{3k_{22}}{4k_{11}} - \frac{k_{11}}{4k_{22}}; b = \frac{1}{2} + \frac{3k_{11}}{4k_{22}} - \frac{k_{22}}{4k_{11}} \quad (6)$$

3.2 Flexodomains under simultaneous dc and ac fields

A simple technique of estimating k_{ii} and e^* employs experiments involving joint action of dielectrically stabilizing ac and flexoelectrically destabilizing dc fields.[40–42] We present in Fig. 5 the dc threshold V_{dc} as a function of V_{ac} for 11Cl at $T^* = 0.989$. In obtaining these data, as in ref. 40–42, the sample was first subjected to a gradually increasing dc voltage till reaching $V_{dc1} = V_c$ at which the flexodomains formed; then, keeping V_c constant, an increasing ac voltage was applied till reaching V_{ac1} that completely suppressed the flexodomains; again, with V_{ac1} fixed, the dc voltage was elevated till reappearance of the domain pattern at V_{dc2} corresponding to V_{ac1}. This procedure was repeated for increasing voltages. Under one elastic constant approximation, it has been shown[40] that V_{dc} varies according to:

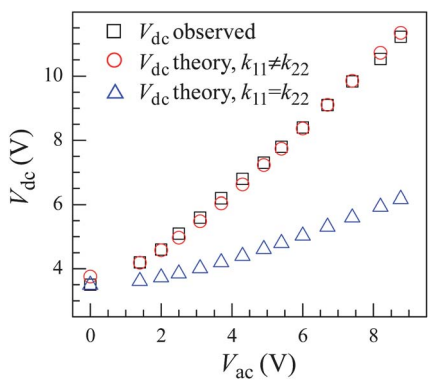

Fig. 5 The variation of dc threshold V_{dc} at which the Bobylev–Pikin flexoelectric domains appear as a function of simultaneously acting ac voltage V_{ac} of frequency 5 kHz. The circles and triangles are theoretical fits under anisotropic and isotropic elasticity, respectively. Squares are the experimental points; $T^* = 0.989$.

It is possible to find values of V_{dc} from eqn (6) that closely match the corresponding experimental values by suitably choosing (k_{11}, k_{22}, e^*) for a given ε_a. However, we find that this choice is not unique. In an attempt to overcome this problem, we undertook to determine (k_{11}/k_{22}) from the geometry of wall defects. For this purpose, we prepared a homeotropic sample of 11Cl with the initial director $\mathbf{n} = (0,0,1)$, and subjected it suddenly to an ac voltage of amplitude well above the Freedericksz threshold $V_F = \pi\sqrt{k_{33}/\varepsilon_0\varepsilon_a}$. In the bend Freedericksz state, the rotational symmetry of the initial structure is broken by the director tilt β with respect to z. The tilt, which reduces from its maximum value in the midplane to zero at the substrates, can occur in any vertical plane since all such orientations are degenerate in terms of free energy and can occur with equal probability. However, the local substrate conditions may often be such that the tilt plane, or equivalently the inplane director $\mathbf{c}$, is not arbitrary; for example, $\mathbf{c}$ may lie along or opposite the direction of capillary flow associated with sample filling. The transitional zone between two such opposite tilt regions constitutes the so-called Brochard–Leger (BL) wall.[43,44] Sections of the wall in the tilt plane are of splay–bend type and those with their normal in the tilt plane are twist–bend. In Fig. 6, we see a metastable closed BL wall formed between regions of opposite tilt in the yz plane. As pointed out very early by Brochard,[43] in the bend Freedericksz state, the equilibrium geometry of closed walls, obtained through minimization of the cyclic integral of wall-energy per unit length, is an ellipse with a, the semimajor axis, $\sqrt{(k_{11}/k_{22})}$ times b, the semiminor axis. Further, closed walls, though irregular in form to begin with, are unstable and, during their spontaneous collapse, assume the equilibrium shape. The rate of collapse $s = da/dt$ along the major axis, obtained by balancing the energy loss due to friction against the energy gain from size reduction, is $s = k_{11}/(\gamma_1 a)$, where γ_1 is the rotational viscosity. For the wall in Fig. 6, we found the average value of

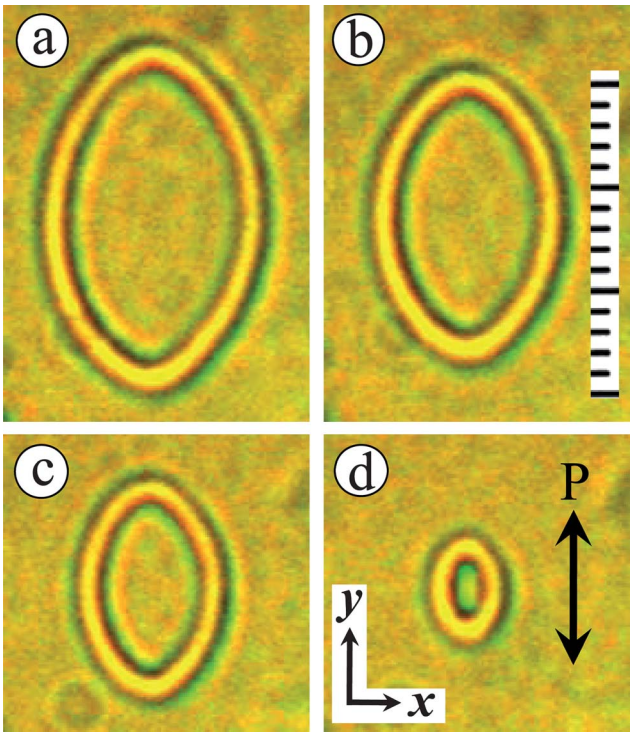

Fig. 6 Time images of a collapsing elliptical Brochard–Leger wall formed in a 15 μm thick, homeotropically aligned nematic layer of 11Cl at $T^* = 0.989$, 1 kHz, 2.06 V_c. Single polarizer (P) set along y. The bright elliptical loops are the focal lines formed by the extraordinary light through the wall. 2 μm scale div. Interval between successive frames is 14 s.

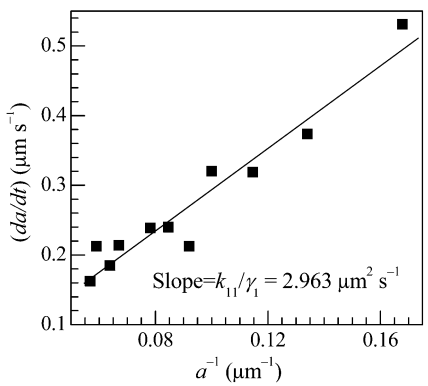

Fig. 7 Rate of decrease in a, the semi-major axis of an elliptical loop wall, as a function of a^{-1}; $T^* = 0.989$.

a/b to be 1.58, which corresponds to $k_{11}/k_{22} = 2.5$. Further, the function $s(a^{-1})$, as seen in Fig. 7, is linear within experimental fluctuations (the coefficient of determination $R^2 = 0.9203$), with a slope corresponding to $k_{11}/\gamma_1 = 2.96$ μm^2 s^{-1}. With $k_{11}/k_{22} = 2.5$, eqn (6) gives the best fit to the experimental data on $V_{dc}(V_{ac})$ in Fig. 5 for $k_{11} = 4.5$ pN, $k_{22} = 1.8$ pN and $|e^*| = 7.95$ pC m^{-1}. Then γ_1 turns out to be 1.52 Pa s, which is of the correct order considering the rotational viscosity data on nCN.[19,20]

Notwithstanding these points of agreement, the fitted values in eqn (6) are to be taken with some caution since the V_{dc} expression to which eqn (6) reduces under $V_{ac} = 0$ has been shown to be at variance with the more precise expression in ref. 37:

$$V_c^2(q_c) = \frac{(q_c^2+1)^2 - \delta k^2 (q_c^2-1)^2}{q_c^2 + \upsilon[q_c^2 + 1 + \delta k(q_c^2-1)]};\ \delta k = \frac{k_{11}-k_{22}}{k_{11}+k_{22}} \quad (7)$$

where υ is the same as μ in eqn (1) in which k is replaced by its average $k_{av} = (k_{11} + k_{22})/2$. We incorporated our experimental data on k_{11}/k_{22}, V_c ($=V_{dc}$ for $V_{ac} = 0$) and q_c in eqn (7) and found $k_{av}/(e_s - e_b)^2$ to be 5×10^{10} N m^2 C^{-2}, compared to 3.3×10^{10} N m^2 C^{-2} from the fit to eqn (6). As a more exact theoretical treatment of the problem involving simultaneous action of ac and dc is presently unavailable, we cannot better specify the accuracy of the flexoparameters derived from eqn (6).

We may also note some of the effects not taken into account in the existing theoretical descriptions of the flexodomain instability that render measurement of flexocoefficients less accurate. First, the field gradients which may exist are ignored and field homogeneity is assumed. Second, in the case of a static field, the observed threshold may be higher than the actual threshold because of voltage induced diffuse counterion layers formed next to the electrodes, which so modify the field that it is homogeneous but lowered in the bulk, and rapidly increasing toward the electrodes in the Debye-like screening layers.[45] When blocking (or aligning) layers are used, the bulk field uniformity is preserved; in this case, selective adsorption of ions of the same sign at these layers could lead to a permanent surface field asymmetry; differential mobility of the opposite charge carriers also produces a similar field change, except that the surface field asymmetry is now transient.[46] Charge injection, which is likely when no blocking layers are applied to the electrodes or when blocking is imperfect, will only render the surface field asymmetric, leaving the bulk field uniform.[47]

3.3 Voltage–domain density and temperature–threshold variations

An important characteristic of the BP domains illustrated in Fig. 8 is the decrease of domain width with increasing voltage, which is the reason for referring to the instability as the VGM. Theoretically, it has been shown that the spatial period of the domain structure in the nonlinear distortion regime is given by:

$$\lambda = \frac{\pi k d}{0.6 e' V'} \quad (8)$$

provided $\varepsilon_a = 0$, $e_s = -e_b = e'$ and $k_{ii} = k$; this result has been noted as qualitatively valid even when $\varepsilon_a \neq 0$, $e_s \neq -e_b$ under the condition $|\mu| < 1$.[34,36] For the best fit in Fig. 5, $|\mu| = 0.246$. Thus the domain density $\kappa = 1/w$ is expected to scale directly as the voltage for fixed values of T and d. In Fig. 9 we present the dependence of κ on V, which is expectedly linear. In fact, a similar behaviour has long since been known in several nematics.[32,33,48–50] However, 11Cl differs from several other nematics with regard to temperature variation of V_c. From eqn (1), it is clear that V_c should vary with temperature in the same manner as k/e^*. For an azoxy compound, Barnik *et al.*[50] have found V_c to be almost temperature independent; they explain this as due to identical temperature variations of k and e^*. However, for 11Cl, we find the temperature coefficient of threshold to be negative, and pronouncedly so close to T_{NI}, as in

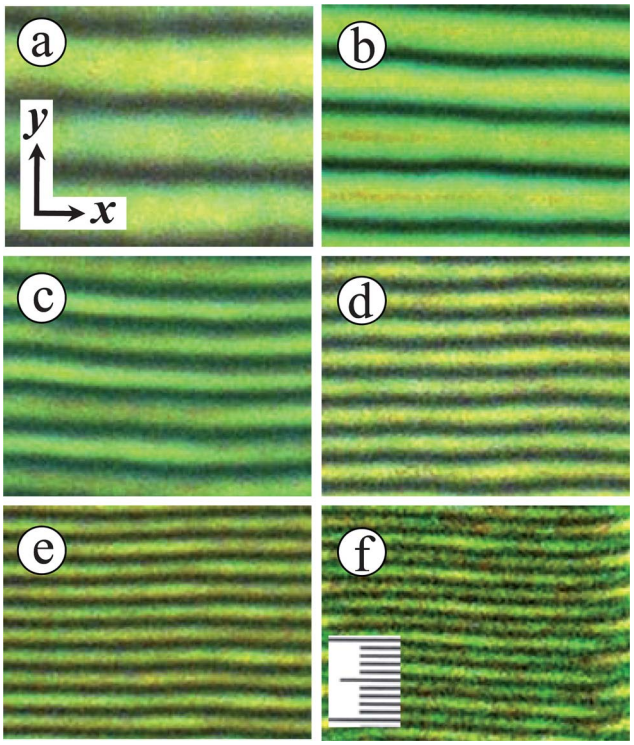

Fig. 8 Increasing density of Bobylev–Pikin domains under an increasing dc field in 11Cl at $T^* = 0.994$. Voltages in units of V_c: (a) 1.07, (b) 1.32, (c) 1.78, (d) 2.21, (e) 2.71 and (f) 3.57. Crossed polarizers set along (x, y); 1 μm scale div.

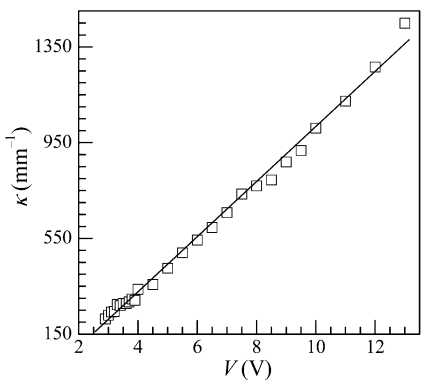

Fig. 9 Flexoelectric domain density as a function of applied voltage for a 5.5 μm thick sample of 11Cl at $T^* = 0.989$; κ^{-1} represents the separation between adjacent extinction lines of the flexo-pattern observed with the polarizer and analyzer set along and transverse to the easy axis.

Fig. 10. It is known that k is quadratic in the order parameter S (T); further, from the molecular theory of dipolar flexoelectricity,[51] e_s and e_b are expressible, respectively, as $[AS^2(1 + 2S)/T]$ and $[BS^2(1 + S/2)/T]$ where A and B are constants involving components of dipole moment and shape anisotropy of molecules appropriate to splay and bend deformations. Therefore, we have

$$\frac{k}{|e^*|} \propto \frac{T}{\left|(A-B) + \left(2A - \frac{B}{2}\right)S\right|'} \tag{9}$$

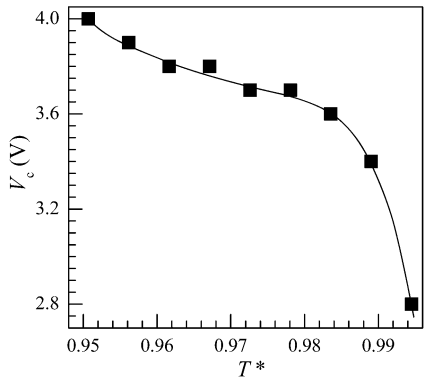

Fig. 10 Temperature variation of the threshold voltage for the Bobylev–Pikin flexoelectric domains instability.

and the behaviour in Fig. 10 is quite the opposite of what this equation predicts. Another factor to consider here is the anisotropy of elastic coefficients; for compounds with $\varepsilon_a < 0$, theoretically, V_c should show a monotonic increase with k_{22}/k_{11}.[36] This is readily seen from eqn (6) where $V_{ac} = 0$, and k_{22} is varied keeping k_{11} and e^* fixed. Thus, a sufficiently negative temperature coefficient of k_{22}/k_{11} could explain the trend in Fig. 10, but this cannot be confirmed at present due to nonavailability of data on k_{22}/k_{11} as a function of T for 11Cl or any of the compounds nX. For calamitics, in many cases, k_{22}/k_{11} varies only marginally with T, and also this variation could be increasing or decreasing.[18] Finally, some calamitic nematogens have been observed experimentally to show a negative temperature coefficient of k/e^*, with e^* varying more like S than S^2; this behaviour has been attributed to a relative increase in the number of conformations producing bent structures with elevation in temperature.[52]

3.4 Pattern morphology under increasing field

When the applied field is enhanced slightly from threshold E_c to E, the optimum wave vector needs to change from q_c to $q > q_c$. This domain compression, if the periodic modulation were to remain defect free, would require large scale director reorientations and high energy. In other words, a considerable stress σ_{yy} would develop on retaining the initial periodicity.[36] This situation is obviated by the generation of dislocations and concomitant decrease in the effective period. Dislocation comprises an additional optical domain or an extra pair of adjacent domains originating or terminating at a point along x (Fig. 11). Such defects are similar to edge dislocations in the layered order of Sm liquid crystals, which are in effect a combination of a pair of opposite disclinations.[53] The topological charge N associated with a dislocation may be defined generally as:

$$N = \frac{1}{2\pi}\oint \mathbf{k}.\mathbf{ds} = \pm 1, \tag{10}$$

where $\mathbf{k}$ is the local wavevector normal to the domain axes and given by the local gradient of the phase variable, $\nabla\psi$; ψ is linear in y in the defect free periodic domain state. While computing the cyclic integral around a defect in the anticlockwise sense as in Fig. 11a, the + sign applies to the dislocation with the additional

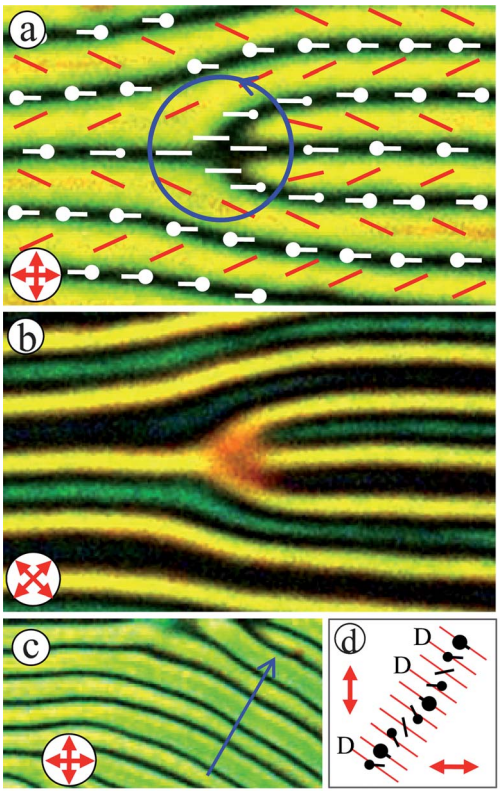

Fig. 11 (a) A positive edge dislocation of unit strength formed in the flexoelectric domain structure at $T^* = 0.989$, $V = 1.15\ V_c$. Red arrows indicate the polarizer–analyzer setting. The dark fringes delineate pure tilt planes or vertical sections to which the director is confined. They turn bright for diagonally crossed polarizers as in (b) showing the same region; the orange-red colour seen at the dislocation in (b) is the same as the birefringence colour of the base planar state. The director field corresponding to the observed domain pattern is shown schematically in (a) by white pins indicating out-of-layer plane tilts and red lines indicating in-plane azimuthal deviations; it conforms to the Bobylev–Pikin model. (c) Double periodicity of the extinction lines in a region where the wavevector (blue arrow) is oblique. (d) Director field for the oblique domains; thin red lines are equi-inclination lines; black nails and lines represent the molecules; extinction lines are indicated by 'D'.

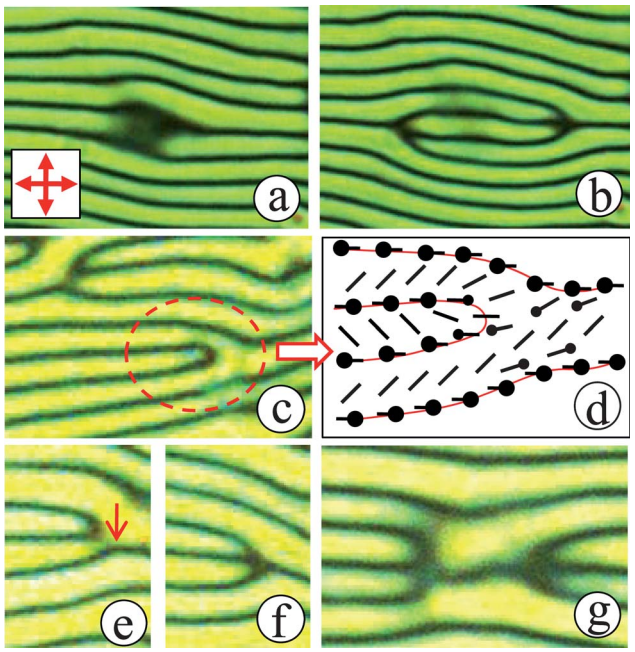

Fig. 12 Defects in the BP domain structure above the threshold voltage, at $T^* = 0.994$. (a) Nucleation of an edge dislocation pair following a long wavelength perturbation at $V = 1.21\ V_c$; (b) same region showing well formed and farther separated defect pair at $V = 1.25\ V_c$; the director field corresponding to these defects (t-dislocations) has a tilt deformation plane common to the extra pair of domains, as seen in Fig. 11a. (c) A second type of dislocation (a-dislocation) seen within the dotted ellipse has an azimuthal deformation plane common to the extra pair of domains, as depicted schematically in (d). (e and f) Conversion of an a-dislocation into t-dislocation *via* glide. (g) A pair of oppositely charged t-dislocations along the same line before annihilation.

domain pair to the right. In Fig. 11a, the oblique red lines between the dark bands indicate the director azimuthally deviated in the layer midplane; the white pins represent the director tilted in the xz midplane, and the white lines denote the undisturbed director at the defect site. We note that, unlike at Sm edge dislocations where singularities appear in the director distribution, at flexostructural defects the director field lines are continuous. The rise in birefringence color at the defect site corresponding to this director field is evident in Fig. 11b. Fig. 11c depicts the double periodicity of extinction lines in the region of oblique domains (discussed later); this is explicable from the director field shown in Fig. 11d.

In Fig. 12a and b, we illustrate the process of evolution and subsequent drifting apart of two paired dislocations under a gradual field elevation. Here, by 'pairing' we mean that, of the two domains associated with each dislocation, one is common to the two dislocations. The domains, which are initially rectilinear, first become unstable against a long-wavelength undulatory perturbation under increased stress. This effect is analogous to the thermally induced layer undulation instability in the Sm C phase[54] derived from the Sm A phase. It is attributed to the tilting of the director away from the layer normal in the course of the phase transition; the resulting large dilatory stresses, in the absence of nucleation of new layers, lead to the undulations. Here, under increasing field, the attendant decrease in domain width leads to such stresses as are relieved through undulations in the absence of nucleation of new domains. These undulations are eventually relaxed by the nucleation of edge dislocation pairs at higher voltages, as exemplified in Fig. 12a. With further increase in V, the − and + defects drift more and more along $+x$ and $-x$ directions, respectively (Fig. 12b) so that an overall increase in the wavenumber results. The extra optical domain or the 'half-layer' of a dislocation may contain along its median either a polar tilt plane (p-dislocation) as in Fig. 12b or an azimuthal tilt plane (a-dislocation) as in Fig. 12c (corresponding to the director field in Fig. 12d). Energetically, p-dislocations seem to be preferred, since a-dislocations transform to p-type during dislocation motion. This is demonstrated in Fig. 12e and f wherein the defect motion is predominantly glide. When the wavevector is along y, the defects generally exhibit climb motion rather than glide. In Fig. 12g we see a pair of opposite p-dislocations prior to their annihilation through climb. Sometimes, as in the relaxation of Sm layers subjected to a uniform dilatory

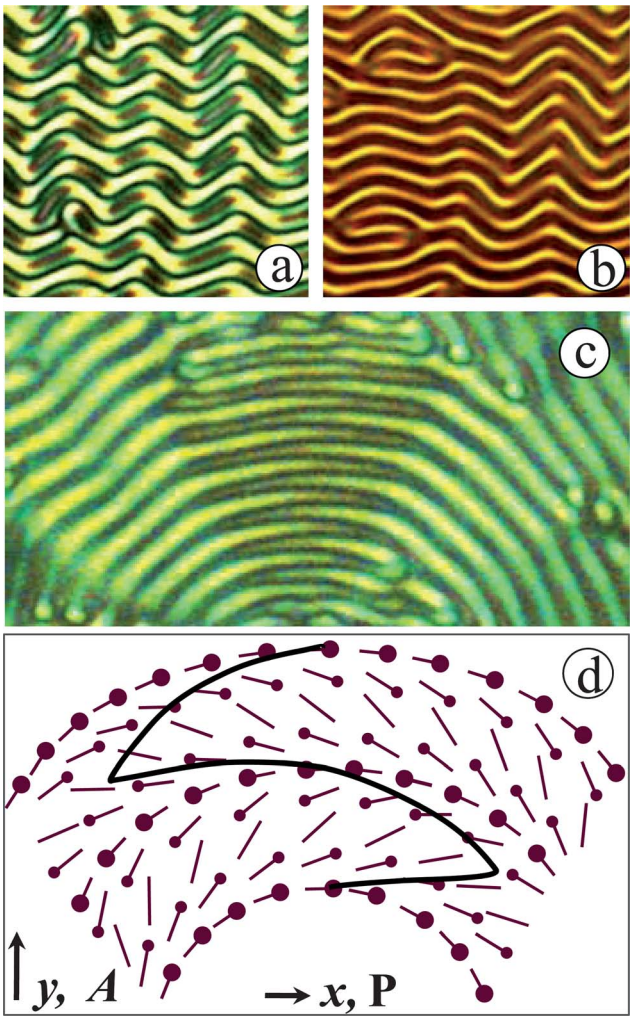

Fig. 13 (a and b) Undulatory instability developed at $V = 1.47\ V_c$ and $T^* = 0.989$; crossed polarizers along (x, y) in (a); single polarizer along x in (b). (c) Circular domains formed around a disturbed alignment zone as seen with crossed polarizers along (x, y), showing a zigzag extinction line. (d) Director configuration corresponding to (c) wherein the black zigzag line represents the extinction path.

stress *via* the undulatory instability, the longitudinal flexodomains may develop a curvature deformation as in Fig. 13a and b. This is a striking feature not having an analogue in the flexostructure of calamitics and indicative of the relative ease with which a bend deformation can enter the distortion initially composed only of splay and twist. When the domains are strongly curved, under crossed polarizers, they display a characteristic zigzag extinction line along y, as shown for the semicircular domains in Fig. 13c. The origin of this line is clarified in Fig. 13d depicting the corresponding director field. Here, the azimuthal midplane tilts are predominantly along x at top left and bottom right, and predominantly along y at top right and bottom left. Corresponding to the latter case, there exists across the sample thickness an inplane twist with an effective pitch $p = 2d$; however, we find light leakage through crossed polarizers since the Mauguin waveguiding condition, *i.e.*, $\Delta np \gg \Lambda$, is not adequately satisfied.

Since flexomodulations involve both polar and azimuthal deviations of the director, they are optically visualizable either by shadowgraphic imaging or through interference of polarized light. When using a single polarizer, they are seen for all orientations of the incident light vector. The focusing of light is due to periodic θ modulation that leads to a corrugation of the extraordinary planar wave surface incident on the sample; as in the case of the Williams domain mode,[55] the flexodomains may be regarded as an array of cylindrical lenses for the extraordinary component of light incident perpendicularly on the layer; the emergent nonparallel rays generate an array of cusped caustics with the cusp lines now along x.[56] In effect, a succession of focal planes form on both real and imaginary sides for each wavelength. For mercury green light, from a series of z-stacked images, we have found three distinct focal planes on either side of the sample midplane. When white light is used, due to dispersion of birefringence, we find colour separation in the z-stacked images. In Fig. 14, we present a few of the coloured line images formed in real space by the flexo-lens system corresponding to a domain width of about 2 μm. For a rough estimate of the focal power f^{-1}, we may employ the same expression as derived early by Carroll[57] for Williams domains: $f^{-1} = \Delta n d\theta_o^2 q^2$, where θ_o is the maximum or midplane value of θ. For argument, if we suppose Δn to vary between 0.09 and 0.07 for increasing wavelength in the visible region, and take $d = 5.5$ μm, $\lambda = 4$ μm and $\theta_o = 30°$, we find f to vary correspondingly in the range 3–3.8 μm. The change Δf in f is too small for resolution of the first focal planes of different wavelengths, and a system of variously coloured bands is seen as a net effect in Fig. 14a showing the real image at 3 μm from the sample midplane. With increasing Δf for higher focal planes, the crowding of colours reduces, as in Fig. 14b and c.

The analogy between a Sm A liquid crystal and a BCN like 11Cl in the BP state can be extended to the problem of interaction between parallel edge dislocations. It is known that, in the first case, the force on a given dislocation due to the stress field of

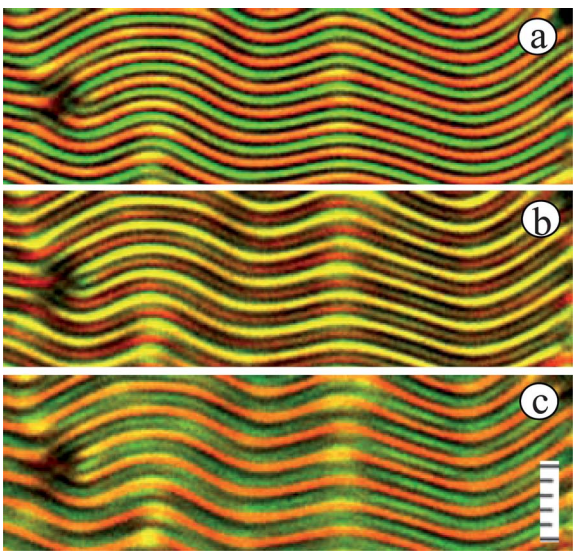

Fig. 14 Colour separation by flexodomains acting as an array of liquid crystal lenses with wavelength dependent power; illumination with white light polarized along y; no analyzer; the microscope stage is raised toward the objective from (a) to (c) above the sample midplane. Separation between images is 3 μm, with (a) at ~3 μm from midplane; 1 μm scale div.

a neighbouring dislocation is obtained by the Peach–Koehler equation.[58] If (F_x, F_z) are the components of force along and normal to Sm planes, between like defects, F_x is always repulsive, while F_z is either attractive or repulsive depending on the location of one defect relative to the other. This explains the 'clustering' of like dislocations in the domain wall between contiguous Sm 'grains'. In a like manner, two neighbouring regions of flexo-bands with their wavevectors at a slight angle are often bridged by a narrow region of like dislocations. This is illustrated in Fig. 15a–d. Fig. 15a shows the texture under birefringence contrast. The patterns in Fig. 15b–d are obtained using a single polarizer; since a strong focussing effect occurs at defect sites for the component of light polarized along x, the defect sites appear as bright spots in the real focal plane as in Fig. 15d, and they are dark in the virtual plane, as in Fig. 15c. Occurrence of a chain of dislocations of the same sign along a common extinction line separating two wavevector regions, as seen in Fig. 15e, is less common compared to branching of dislocations as in Fig. 15a–d. Another less common stable configuration of dislocations is depicted in Fig. 15f; here defects of opposite polarity are stacked alternately along y.

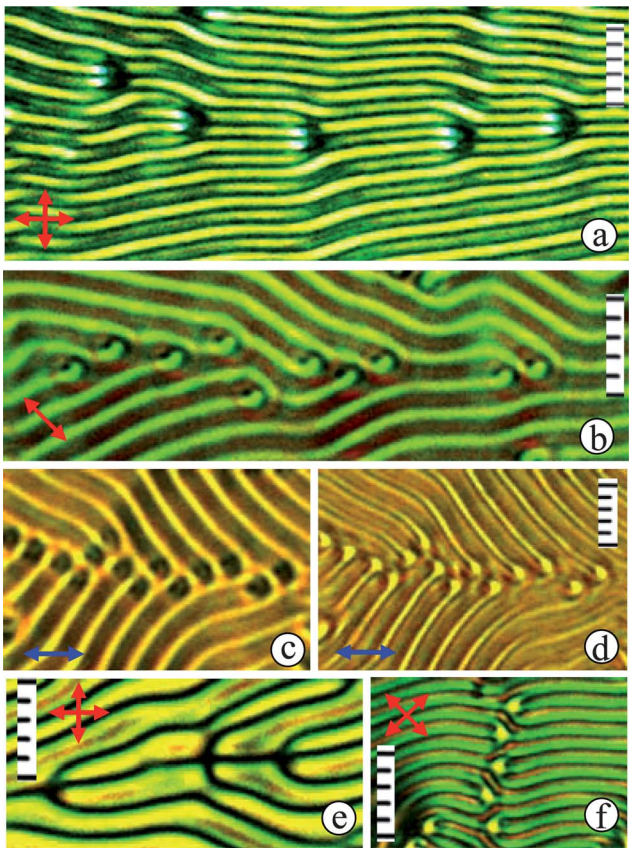

Fig. 15 (a–d) Clustering of like dislocations at the 'boundary' between two flexodomain regions with the wavevectors at a slight angle. The double-headed arrows indicate the orientation of polarizers. Textures in (c) and (d) are of the same region in the virtual and real focal planes, respectively. (e) Uncommon succession of dislocations of the same sign along the line of separation between two wavevector regions. (f) Alternately positive and negative dislocations formed along y; 2 μm scale div. Voltages in units of V_c: (a) 2.07, (b) 2.86, (c and d) 2.06, (e) 1.45 and (f) 2.06; $T^* = 0.994$ for (a and b) and 0.989 for (c–f).

The curvature distortion of domains is often a consequence of the formation of a network of edge dislocations. The climb motion of dislocations occurring along the domains under field elevation may impose such curvature changes as will eventually lead to a chevron-like morphology. In Fig. 16a–c exemplifying this feature, edge dislocations in the upper half are at the boundary between two regions of differently oriented domains. While generally moving to the left with voltage rise, they also slide down because of the sloping boundary, causing the domains underneath to undulate. The net result of these modulations is the chevron texture in Fig. 16c. Fig. 16d shows a region of extensive chevron formation under crossed polarizers; the defects

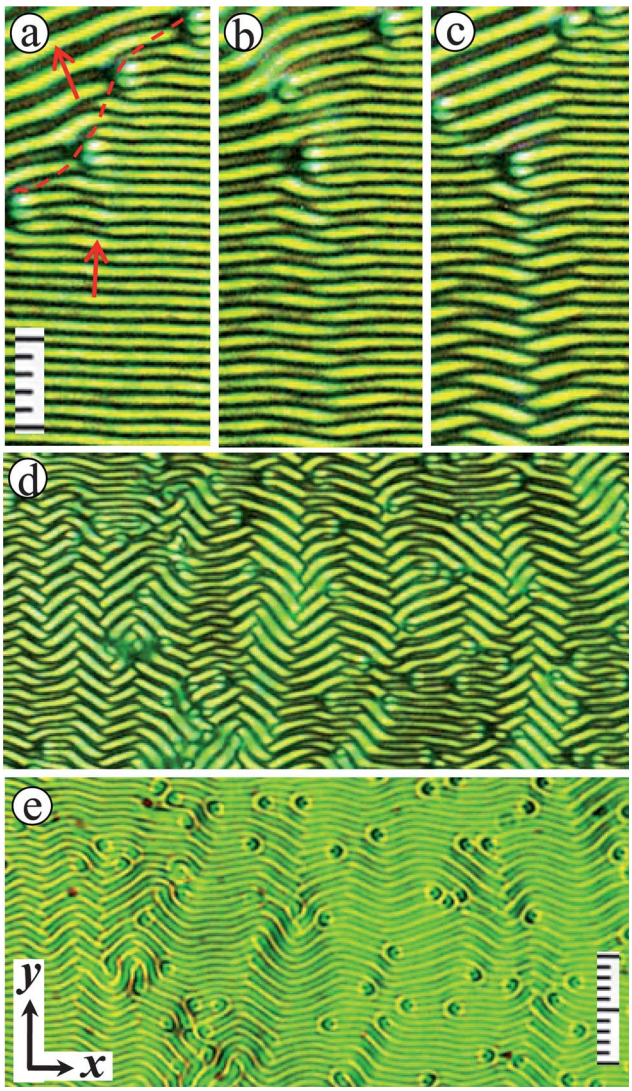

Fig. 16 Chevron-like texture formed under increasing voltage through motion of defects at the boundary indicated by the dotted red line separating different wave vector (red arrows) regions; 5.5 μm thick sample at $T^* = 0.994$. Voltages in units of V_c: (a) 2.14, (b) 2.21, (c) 2.28 and (d and e) 2.5. For (a–d), crossed polarizers along (x, y), and for (e) single polarizer along x. (d) and (e) show the same region. 5 μm scale div; same magnification for (a–c), and for (d and e). The edge dislocations at the boundary slide down while climbing with increase in voltage, causing the domains underneath to undulate.

are vividly revealed in Fig. 16e showing the same region, now observed with a single polarizer.

The appearance of flexodomains in the high field regime bears a striking resemblance to that of a long pitch cholesteric under homeotropic boundary conditions. In the latter case, the orientation of the twist axis is degenerate in that it can be along any line in the plane of the sample; in practice, this orientation varies smoothly over large distances to result in an optical texture which, under crossed polarizers, consists of variously curving parallel dark lines separated by half the pitch length; the director or the optical axis is evidently transverse to the substrates along the extinction lines of this so-called 'fingerprint' pattern. We present in Fig. 17 a high field texture of 11Cl that is quite like the cholesteric fingerprint texture. It contains, besides numerous edge dislocations, several π-disclinations of opposite sign. The nearly parabolic cusp line (in red) in Fig. 17, though reminiscent of a parabolic focal conic defect line, is actually a horizontal section of a vertical parabolic sheet. We present in Fig. 18 the textures that demonstrate the evolution of singular line defects around which the domains curve in a manner that the parabolic cusp sheets are generated. When the undulatory domains are subjected to further increase in electrical stress, they tend to become zig-zag. Thus the continuous change in the wavevector component along x between positive and negative values gives way to a discontinuous switchover when the undulations become sharply peaked. This results in a tilt-wall like structure that eventually undergoes pincement (Fig. 18d), just as a BL splay–bend wall,[43,44] resulting in the appearance of two opposite line defects of strength $^1/_2$, which are transverse to the layer plane and laterally separated along y. The domains seen with a single polarizer may appear to be discontinuous in the vicinity of line

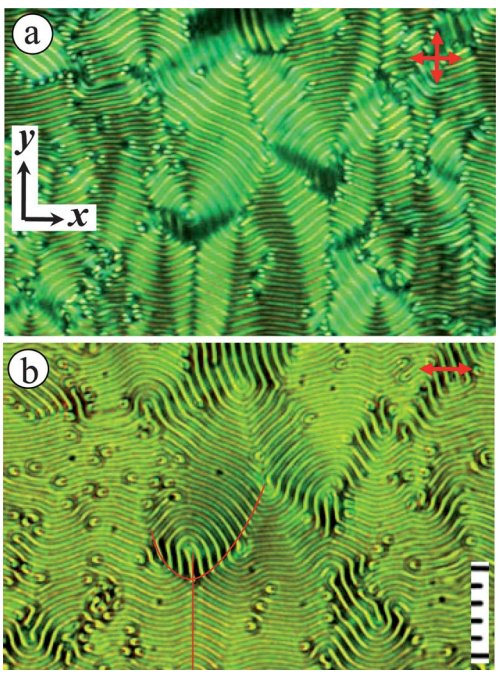

Fig. 17 Cholesteric-fingerprint-like texture at $T^* = 0.994$, $V = 2.9\ V_c$; same region observed with (a) crossed polarizers (red arrows) along (x, y) and (b) single polarizer along x. Red parabolic hairline traces the path along which the domain curvature changes sharply; 5 μm scale div.

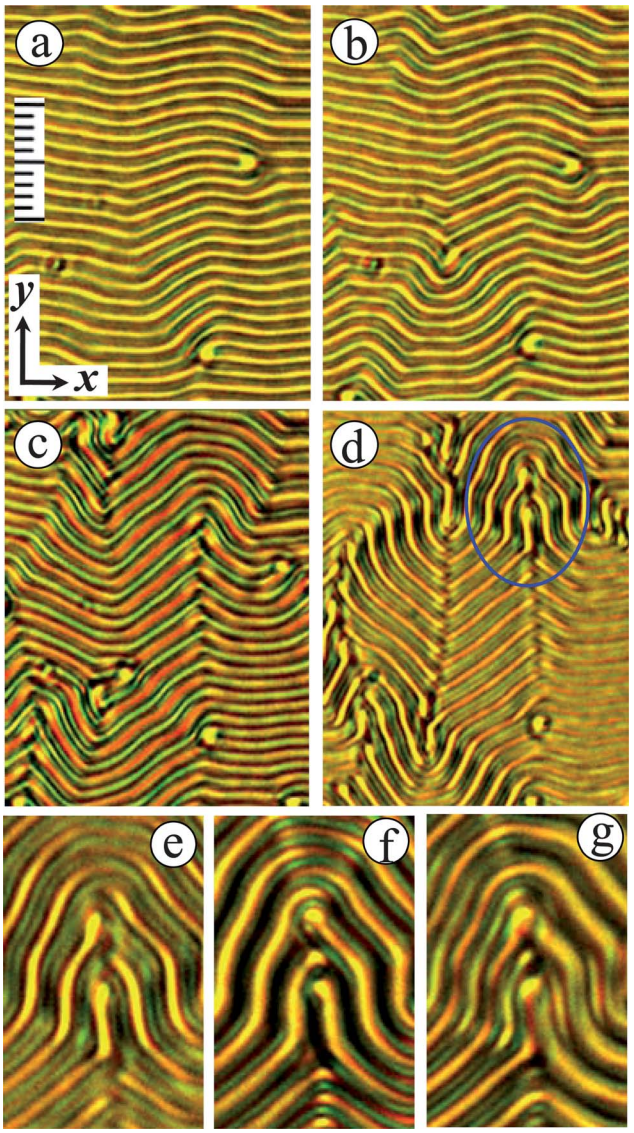

Fig. 18 Development of zigzag domains into pinched walls along y on subjecting the undulation state to increasing electrical stress. Voltages in units of V_c: (a) 1.65, (b) 1.71, (c) 1.86 and (d) 2.12. Single polarizer along x. $T^* = 0.989$; 2 μm scale div; common scale (a–d). (e–g) Enlarged view of the encircled region in (d); single polarizer along x, y and diagonal directions in (e), (f) and (g), respectively. The apparent discontinuities in domain lines at the U-turn in (e and f) are due to polarization dependent focusing. The strongly focused line images in (e) and (f) are along the complementary sides of the bend. Pincement involves the creation of a pair of oppositely charged $^1/_2$ -strength disclinations, which here are of τ type.

defects, as in Fig. 18d, because of polarization dependent focusing. That this is not the case is evident from Fig. 18e–g. The molecular orientation pattern around the line defects may be visualized as in Fig. 19a. Since the defect lines here are perpendicular to the local molecular axis, they may be regarded as τ-type. It may be noted that, unlike in cholesterics, we cannot have a λ-disclination here as the director cannot be along z all across the sample under strong planar anchoring.

The flexostructure can be considered a lattice of periodicity equal to the domain width in the same way a cholesteric may be

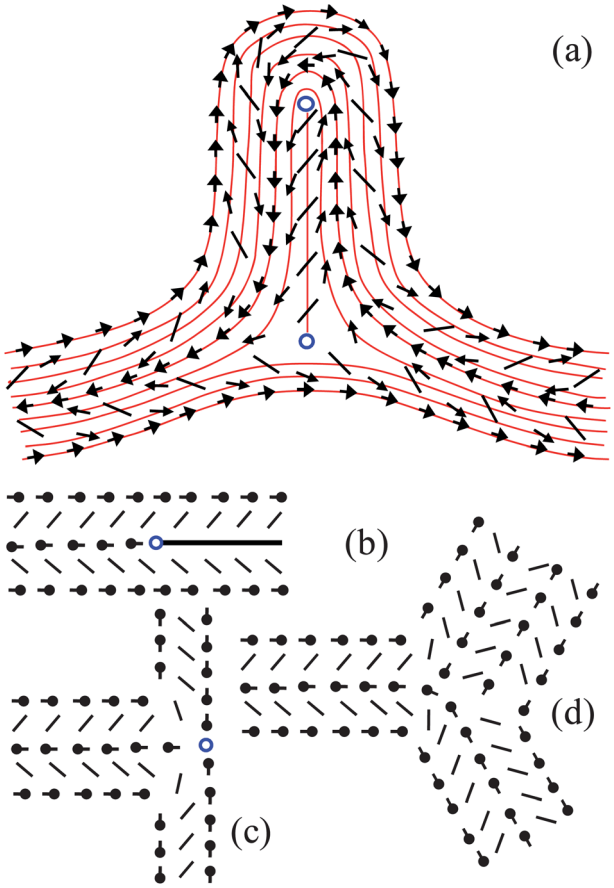

Fig. 19 (a) Director configuration around a pair of oppositely charged $^1/_2$ strength defects resulting from pincement. Here the red lines are the equal inclination contours, arrows indicate out-of-plane tilts, and blue circles are the positive (top) and negative (bottom) defect sites. (b–d) Creation of an imperfect negative π-disclination in the flexostructure by the Volterra process.

considered a layered structure of periodicity $P/2$. As in smectics or cholesterics, disclinations may be created in the flexolattice using the Volterra[59] process. In this context, it is helpful to recall the possibilities for a perfect rotational π-disclination of either sign in a Sm A lattice, as discussed by Friedel and Kleman.[60] The rotational symmetry of the liquid crystal here is described by two twofold axes: both are perpendicular to the molecules, but one of them passes in-between two layers while the other is located in the middle of a layer. Thus, the cut surface involved in the Volterra process may be positioned either at the end or in the middle of a Sm layer. Correspondingly, we obtain two types of π-disclination of a given sign, referred to as Ω_a and Ω_b. In the case of flexolattice, we have only one twofold axis that passes through a φ-only plane, midway between two tilt planes. This explains our molecular model for the oppositely charged pair of perfect τ disclinations in Fig. 19a. A perfect disclination may glide parallel to itself and turn into an imperfect defect. A glide, for example, of a τ^- by a distance $\lambda/4$ along the wavevector is, in effect, the result of choosing the Volterra cut through a θ-only plane. This is exemplified in Fig. 19b–d. In Fig. 19b, the cut surface Σ coinciding with a tilt plane terminates along what is to be the singular line L parallel to y. The two half-planes from the cut are then rotated oppositely about L through π/2, as in Fig. 19c; the director tilts in the upper and lower parts of the boundary are now opposite. Therefore, the two half planes are rotated toward each other sufficiently to match the perfect lattice added on the right side. This results in the structure in Fig. 19d that corresponds to an imperfect defect. Since a slight reorganization of the core of this defect converts it into a perfect τ^- disclination, we may consider it an excited state of τ^-.

The disclinations of the high field flexostructure are often found to be organized in various patterns, the likes of which are well known in long pitch cholesterics.[61] Fig. 20 provides some examples of such patterns. In Fig. 20a–c, the positive and negative τ defects are seen forming a zig-zag chain. Similarly, in Fig. 20d–f, angular quadrupoles, consisting of two positive and two negative π-disclinations at the corners of a quadrilateral, are

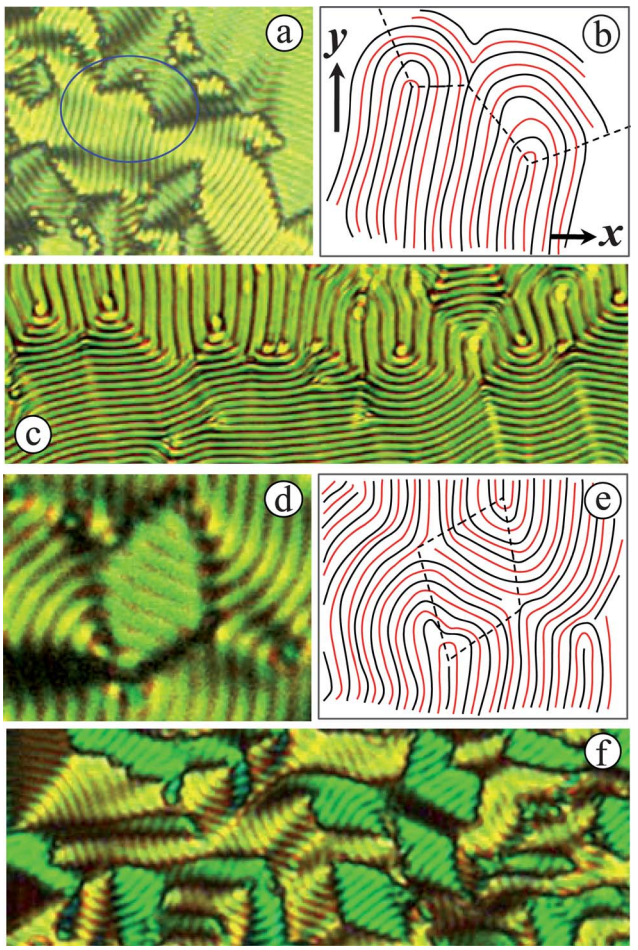

Fig. 20 Various patterns formed by τ^+ and τ^- disclinations in the flexodomain structure. (a) Zig-zag extinction lines seen under crossed polarizers; they join positive and negative defects occurring alternately at the turning points. (b) The director field corresponding to the encircled region in (a); the black and red lines are along the dark and bright bands of the pattern. (c) An array of alternately positive and negative π-disclinations as seen with a single polarizer along y. (d) Angular quadrupole due to two positive and two negative π-disclinations at the corners of a quadrilateral. (e) The director field corresponding to the texture in (d); the black and red lines are along the dark and bright bands of the pattern. (f) A network of quadrupoles as seen using crossed polarizers with a full-wave plate.

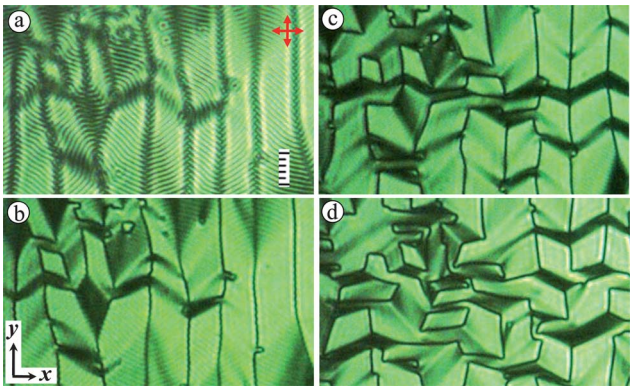

Fig. 21 Textures in the same sample region under crossed polarizers (red arrows), showing the progressive development of the fans (lozenges) with increasing voltage at $T^* = 0.994$. $V/V_c = 1.64$ (a and b), 2.04 (c), 2.54 (d). In (a) the focus is on the birefringence bands, while in (b) it is on the cusp lines. In (c), almost the entire region is filled with angular quadrupoles (fans), and close-spaced domains within them are still discernible. In (d), the flexodomains are unresolved; they are also not visualized by a change of focus; 2 μm scale div.

observed. Such quadrilaterals are frequently found with opposite angles of $\pi/3$ or $2\pi/3$. Finally, we show in Fig. 21 the progressive development of the fan texture with field elevation. Fig. 21a and b show a herring-bone or chevron pattern that is exactly like that in a long pitch cholesteric (see Fig. 10d and ref. 60). However, this likeness seems to be superficial since, in cholesterics, chevrons result from parallel 'lines of flare' alternately occurring at the two substrates with the distorted layers arranged obliquely to the substrates; here the curved 'layers' are upright and there are no lines of flare as in smectics or cholesterics. On enhancing the field, as demonstrated in Fig. 21c and d, angular quadrupoles (fans) form in increasing numbers, while the resolution of flexodomains is eventually lost.

4 Conclusions

We have studied the static field driven patterned state in a thin film of the BC compound 11Cl and identified it as corresponding to the Bobylev–Pikin flexoelectric instability from the polarization characteristics of the domains and the linear dependence of domain frequency on the applied field. The relevant flexoelectric parameter derived from the dc threshold as a function of simultaneously acting ac field is of conventional order. Unusually, the effective flexo- and elastic moduli vary with temperature differently. The study reveals uncommon morphological modifications with field elevation. Besides the frequently occurring edge dislocations, the flexostructure is found to develop positive and negative singular, τ-type line defects of strength $^1/_2$, in the high field regime. This is the first observation of such disclinations in any electrically induced patterned state. The course of distortions leading to these defect forms involves bend elastic deformations which are known to be energetically less expensive than splay deformations in a BC system. The intriguing question of how a BC nematic is able to exhibit a fanlike morphology, unlike any calamitic compound, finds an answer in the patterned disposition of the τ-disclinations and associated degeneracy of wavevector direction in the plane of the film. When the field is so high that the resolution of flexodomains is diffraction limited, the fans, which are mostly angular quadrupoles, appear smooth. These experimental observations raise some fundamental questions related to the structure and energetics of flexodefects. For instance, the critical field at which disclinations appear through pincement of the zig-zag domains and the nature of interaction between disclinations underlying the propensity of the topological charges to occur frequently in quadrupolar configurations are interesting problems for future analysis.

Acknowledgements

We thank Professor K. A. Suresh and Dr Praveer Asthana for the experimental facilities, and Academician A. G. Petrov and Dr Y. Marinov for useful discussions. This study is carried out under Project No. INT/BUL/B-75/07, supported by the Department of Science and Technology, New Delhi.

References

1 H. Takezoe and Y. Takanishi, *Jpn. J. Appl. Phys.*, 2006, **45**, 597–625.
2 R. Amaranatha Reddy and C. Tschierske, *J. Mater. Chem.*, 2006, **16**, 907–961.
3 J. Etxebarria and M. Blanca, *J. Mater. Chem.*, 2008, **18**, 2919–2926.
4 T. Niori, T. Sekine, J. Watanabe, T. Furukawa and H. Takezoe, *J. Mater. Chem.*, 1996, **6**, 1231–1233.
5 D. R. Link, G. Natale, R. Shao, J. E. Maclennan, N. A. Clark, E. Körblova and D. M. Walba, *Science*, 1997, **278**, 1924–1927.
6 H. R. Brand and H. Pleiner, *Eur. Phys. J. E*, 2010, **31**, 37–50.
7 G. Pelzl, A. Eremin, S. Diele, H. Kresse and W. Weissflog, *J. Mater. Chem.*, 2002, **12**, 2591–2593.
8 W. Weissflog, S. Sokolowski, H. Dehne, B. Das, S. Grande, M. W. Schröder, A. Eremin, S. Diele, G. Pelzl and H. Kresse, *Liq. Cryst.*, 2004, **31**, 923–933.
9 T. Niori, J. Yamamoto and H. Yokoyama, *Mol. Cryst. Liq. Cryst.*, 2004, **409**, 475–482.
10 V. Görtz and J. W. Goodby, *Chem. Commun.*, 2005, 3262–3264.
11 M. G. Tamba, U. Baumeister, G. Pelzl and W. Weissflog, *Liq. Cryst.*, 2010, **37**, 853–874.
12 O. Francescangeli and E. T. Samulski, *Soft Matter*, 2010, **6**, 2413–2420.
13 C. Keith, A. Lehmann, U. Baumeister, M. Prehm and C. Tschierske, *Soft Matter*, 2010, **6**, 1704–1721.
14 S. H. Hong, *Short-Range Structure of Nematic Bent-Core Mesogens*, PhD dissertation, Kent State University, May 2010.
15 C. Tschierske and D. J. Photinos, *J. Mater. Chem.*, 2010, **20**, 4263–4294.
16 E. T. Samulski, *Liq. Cryst.*, 2010, **37**, 669–678.
17 W. H. de Jeu, *Physical Properties of Liquid Crystalline Materials*, Gordon and Breach Science Publishers, New York, 1980.
18 S. V. Pasechnik, V. G. Chigrinov and D. V. Shmeliova, *Liquid Crystals: Viscous and Elastic Properties*, Wiley-VCH, Weinheim, 2009.
19 P. Tadapatri, U. S. Hiremath, C. V. Yelamaggad and K. S. Krishnamurthy, *J. Phys. Chem. B*, 2010, **114**, 1745–1750.
20 P. Tadapatri, K. S. Krishnamurthy and W. Weissflog, *Phys. Rev. E: Stat., Nonlinear, Soft Matter Phys.*, 2010, **82**, 031706.
21 P. Sathyanarayana, M. Mathew, Q. Li, V. S. S. Sastry, B. Kundu, K. V. Le, H. Takezoe and S. Dhara, *Phys. Rev. E: Stat., Nonlinear, Soft Matter Phys.*, 2010, **81**, 010702.
22 M. Majumdar, P. Salamon, A. Jákli, J. T. Gleeson and S. Sprunt, *Phys. Rev. E: Stat., Nonlinear, Soft Matter Phys.*, 2011, **83**, 031701.
23 E. Dorjgotov, K. Fodor-Csorba, J. T. Gleeson, S. Sprunt and A. Jákli, *Liq. Cryst.*, 2008, **35**, 149–155.
24 J. Harden, B. Mbanga, N. Eber, K. Fodor-Csorba, S. Sprunt, J. T. Gleeson and A. Jákli, *Phys. Rev. Lett.*, 2006, **97**, 157802.
25 J. Harden, R. Teeling, J. T. Gleeson, S. Sprunt and A. Jákli, *Phys. Rev. E: Stat., Nonlinear, Soft Matter Phys.*, 2008, **78**, 031702.
26 A. Jákli, *Liq. Cryst.*, 2010, **37**, 825–837.

27 K. V. Le, F. Araoka, K. Fodor-Csorba, K. Ishikawa and H. Takezoe, *Liq. Cryst.*, 2009, **6**, 1119–1124.
28 P. Kumar, Y. G. Marinov, H. P. Hinov, U. S. Hiremath, C. V. Yelamaggad, K. S. Krishnamurthy and A. G. Petrov, *J. Phys. Chem. B*, 2009, **113**, 9168–9174.
29 F. Castles, S. M. Morris and H. J. Coles, *AIP Adv.*, 2011, **1**, 032120.
30 A. G. Petrov, Private Communication.
31 L. Kovalenko, M. W. Schroder, R. A. Reddy, S. Diele, G. Pelzl and W. Weissflog, *Liq. Cryst.*, 2005, **32**, 857–865.
32 L. K. Vistin, *Sov. Phys. Dokl.*, 1971, **15**, 908–910.
33 W. Greubel and W. Wolf, *Appl. Phys. Lett.*, 1971, **19**, 213–215.
34 Y. P. Bobylev, V. G. Chigrinov and S. A. Pikin, *J. Phys. (Paris)*, 1979, **40**(Suppl. 4), C3:331; Y. P. Bobylev and S. A. Pikin, *Sov. Phys. JETP*, 1977, **45**, 195–198.
35 B. H. Soffer, J. D. Margerum, A. A. Lackner, D. Boswell, Jr, A. R. Tanguay, T. C. Strand, A. A. Sawchuk and P. Chavel, *Mol. Cryst. Liq. Cryst.*, 1981, **70**, 145–161.
36 S. A. Pikin, *Structural Transformations in Liquid Crystals*, Gordon and Breach Science Publishers, New York, 1991.
37 A. Krekhov, W. Pesch and A. Buka, *Phys. Rev. E: Stat., Nonlinear, Soft Matter Phys.*, 2011, **83**, 051706.
38 S. P. Palto, N. J. Mottram and M. A. Osipov, *Phys. Rev. E: Stat., Nonlinear, Soft Matter Phys.*, 2007, **75**, 061707.
39 M. Kleman and O. D. Lavrentovich, *Soft Matter Physics: an Introduction*, Springer Verlag, New York, 2003.
40 Y. Marinov, H. P. Hinov and A. G. Petrov, *J. Optoelectron. Adv. Mater.*, 2005, **7**, 277–280.
41 Y. Marinov and H. P. Hinov, *J. Opt. Technol.*, 2005, **72**, 944–950.
42 Y. Marinov, A. G. Petrov and H. P. Hinov, *Mol. Cryst. Liq. Cryst.*, 2006, **449**, 33–45.
43 F. Brochard, *J. Phys.*, 1972, **33**, 607–611.
44 L. Leger, *Mol. Cryst. Liq. Cryst.*, 1973, **24**, 33–44.
45 G. Barbero, D. Olivero, N. Scaramuzza, G. Strangi and C. Versace, *Phys. Rev. E: Stat., Nonlinear, Soft Matter Phys.*, 2004, **69**, 021713.
46 R. N. Thurston, *J. Appl. Phys.*, 1984, **55**, 4154; R. N. Thurston, J. Cheng, R. B. Meyer and G. D. Boyd, *J. Appl. Phys.*, 1984, **56**, 263–272.
47 S. Lu and D. Jones, *Appl. Phys. Lett.*, 1970, **16**, 484–486.
48 L. K. Vistin, *Kristallografia*, 1970, **15**, 594.
49 J. M. Pollak and J. B. Flannery, in *Liquid Crystals and Ordered Fluids*, ed. J. F. Johnson, and R. S. Porter, Plenum Press, New York, 1974, vol. 2.
50 M. I. Barnik, L. M. Blinov, A. N. Trufanov and B. A. Umanski, *J. Phys.*, 1978, **39**, 417–422.
51 A. I. Derzhanski and A. G. Petrov, *Acta Phys. Pol.*, 1979, **A55**, 747–767.
52 P. R. Maheswara Murthy, V. A. Raghunathan and N. V. Madhusudana, *Liq. Cryst.*, 1993, **14**, 483–496.
53 S. Chandrasekhar and G. S. Ranganath, *Adv. Phys.*, 1986, **35**, 507–596.
54 D. Johnson and A. Saupe, *Phys. Rev. A: At., Mol., Opt. Phys.*, 1977, **15**, 2079–2085.
55 P. A. Penz, *Phys. Rev. Lett.*, 1970, **24**, 1405–1409.
56 E. Plaut, A. Joets and R. Ribotta, *J. Phys. III*, 1997, **7**, 2459–2474.
57 T. O. Carroll, *J. Appl. Phys.*, 1972, **43**, 1342–1346.
58 P. S. Pershan, *J. Appl. Phys.*, 1974, **45**, 1590–1604.
59 M. Kleman, *Points, Lines and Walls*, John Wiley, New York, 1983.
60 J. Friedel and M. Kleman, in *Fundamental Aspects of Dislocation Theory*, ed. J. A. Simmons, R. de Wit and R. Bullough, National Bureau of Standards Special Publication No. 317, Washington DC, 1970, vol. 1.
61 Y. Bouligand, in *Dislocations in Solids*, ed. F. R. N. Nabarro, North Holland, New York, 1980, vol. 5.

